AOS Thesis 2020

Role of Deep Learning–Quantified Hyperreflective Foci for the Prediction of Geographic Atrophy Progression

URSULA SCHMIDT-ERFURTH, HRVOJE BOGUNOVIC, CHRISTOPH GRECHENIG, PATRICIA BUI, MARIA FABIANSKA, SEBASTIAN WALDSTEIN, AND GREGOR S. REITER

• PURPOSE: To quantitatively measure hyperreflective foci (HRF) during the progression of geographic atrophy (GA) secondary to age-related macular degeneration (AMD) using deep learning (DL) and investigate the association with local and global growth of GA.

• METHODS: Eyes with GA were prospectively included. Spectral-domain optical coherence tomography (SDOCT) and fundus autofluorescence images were acquired every 6 months. A 500-μm-wide junctional zone adjacent to the GA border was delineated and HRF were quantified using a validated DL algorithm. HRF concentrations in progressing and nonprogressing areas, as well as correlations between HRF quantifications and global and local GA progression, were assessed.

• RESULTS: A total of 491 SDOCT volumes from 87 eyes of 54 patients were assessed with a median follow-up of 28 months. Two-thirds of HRF were localized within a millimeter adjacent to the GA border. HRF concentration was positively correlated with GA progression in unifocal and multifocal GA (all $P < .001$) and de novo GA development ($P = .037$). Local progression speed correlated positively with local increase of HRF (P value range $<.001$-$.004$). Global progression speed, however, did not correlate with HRF concentrations ($P > .05$). Changes in HRF over time did not have an impact on the growth in GA ($P > .05$).

• CONCLUSION: Advanced artificial intelligence (AI) methods in high-resolution retinal imaging allows to identify, localize, and quantify biomarkers such as HRF. Increased HRF concentrations in the junctional zone and future macular atrophy may represent progressive migration and loss of retinal pigment epithelium. AI-based biomarker monitoring may pave the way into the era of individualized risk assessment and objective decision-making processes. NOTE: Publication of this article is sponsored by the American Ophthalmological Society. (Am J Ophthalmol 2020;216:257–270.

ARTIFICIAL INTELLIGENCE (AI) HAS ARRIVED IN MEDICINE and its implementation into the clinical world is likely to revolutionize daily patient care. Beyond fields such as radiology, dermatology, and pathology, ophthalmology is expected to benefit most strikingly of AI owing to its focus on image-based diagnostics.[1] Together with optical coherence tomography (OCT) imaging,[2] another technological achievement in ophthalmology, AI can reach its full potential and real-time objective and individualized medicine can potentially be provided. The highly organized structures of the retina are an ideal target for implementing AI to support physicians in their work on a daily basis.[3]

Age-related macular degeneration (AMD) affects almost 200 million people worldwide in 2020, which will increase to 288 million in 2040.[4] Clinical classification of AMD differentiates an early and intermediate form, based on the presence of drusen and pigmentary alterations, from 2 late stages, neovascular AMD and geographic atrophy (GA), also called atrophic AMD.[5] In neovascular AMD, new choroidal or retinal vessels develop with clinically present exudation and a rapid decline in visual function.[6,7] GA, on the other hand, is characterized by progressive alteration of photoreceptors and retinal pigment epithelium (RPE) cells, as well as alterations in the choriocapillaris.[8,9] Contrary to neovascular AMD, GA progresses slowly but individually in an unpredictable manner. No medication has yet been clinically approved for the treatment of this form of late-stage disease.[10,11] With innovations in multimodal imaging techniques and in particular OCT, several structural risk factors for the progression from intermediate to late AMD were identified.[12–15] Using machine learning (ML) and including a variety of these risk markers, it is possible to create disease-prognostic "risk signatures" for individual disease progression

Accepted for publication Mar 31, 2020.

From the Christian Doppler Laboratory for Ophthalmic Image Analysis, Vienna Reading Center, Department of Ophthalmology and Optometry, Medical University of Vienna, Vienna, Austria.

Inquiries to Ursula Schmidt-Erfurth, Department of Ophthalmology and Optometry, Medical University of Vienna, Währinger Gürtel 18-20, 1090 Vienna, Austria; e-mail: ursula.schmidt-erfurth@meduniwien.ac.at

with a notable difference between the "risk signature" for neovascular AMD and GA.[16–18] An important feature that is abundantly present in the progression to GA is hyperreflective foci (HRF), a subclinical feature, which can be detected by OCT imaging in high-resolution images.[16,19–21] During disease progression RPE cells overlying a druse either go into apoptosis or migrate into the retina, which results in the formation of HRF and the subsequent collapse of the druse, which cannot sustain its integrity without further RPE functionality.[13,22,23] The collapse of the druse, which starts with the dysmorphia of RPE cells and the subsequent development of GA, is termed the drusen life cycle.[13,24–26] HRF seen on OCT have been demonstrated to be consistent with hyperpigmentary alterations on color fundus photography.[27,28] It is therefore understandable that early classification of intermediate AMD based on color fundus photography mostly relied on the presence and size of drusen and hyperpigmentary alterations, which were also used for individual risk assessment.[29]

While RPE migration alone does not induce vision loss, expanding atrophic lesions do, and disease progression concomitant with visual loss is unhalted. The search for reliable morphologic risk factors that identify and predict lesion growth in GA is therefore actively promoted by many investigators using multimodal approaches.[30,31] In the not-yet-atrophic area adjacent to the edge of the lesion, called the junctional zone, RPE cells show dysmorphia and loss of intracellular fluorophores with already reduced RPE-derived quantitative autofluorescence.[24,32–35] "Junctional zone" is a term that was defined differently in the current literature. Some studies defined the junctional zone on structural alteration (ie, ellipsoid zone loss on OCT), whereas other studies used 1 or several fixed margins around the GA lesion.[33,36–38] The continuous process of RPE degeneration at the junctional zone followed by migration of RPE cells into the overlaying retina allows a novel quantitative biomarker-based assessment using high-resolution 3-dimensional OCT imaging.

Deep learning (DL) is a path of AI that relies on multilayered neural network algorithms that allow the algorithm to learn to extract specific morphologic features on its own. Although DL has to be fed with relatively more data than traditional machine learning, its strength lies in the ability to extract signals that are often invisible to the human expert.[3] Applying DL to retinal image analysis (eg, in OCT), the algorithm requires a dataset of annotated objects, which can be HRF or any other biomarker of clinical relevance. Subsequently, the trained algorithm provides an automated extraction of these image features and can be applied on a new image dataset. To investigate the quantitative impact of HRF on the progression of GA secondary to AMD, a previously built DL model was used to localize and measure the amount of HRF in 3-dimensional OCT images.[39] For this study, we investigate the relationship between spatiotemporal HRF quantification and GA lesion growth to identify the role of HRF in global and local GA progression.

METHODS

• **STUDY DESIGN:** Patients with geographic atrophy (GA) secondary to AMD aged 50 years and over were included in a reported[10,33,40–46] prospective observational cohort study after giving written informed consent. The study was approved by the Ethics Committee of the Medical University of Vienna and adhered to Good Clinical Practice guidelines and the Declaration of Helsinki. Patients with both unifocal and multifocal GA lesions were included in the study. Patients with any signs of neovascular AMD or who had been treated with anti–vascular endothelial growth factor were excluded. Spectral-domain OCT (SDOCT) and fundus autofluorescence (FAF) images were acquired using a Spectralis HRA+OCT (Heidelberg Engineering, Heidelberg, Germany).

• **IMAGING PROTOCOL:** Imaging was performed prospectively using a standardized protocol every 6 months. At least 3 consecutive visits had to be available for inclusion in the analysis. For SDOCT scans, an OCT volume of the central $20 \times 20^{\circ}$ centered on the fovea was acquired with a resolution of 1024×49 (A-scans $\times$ B-scans) using a Spectralis HRA+OCT device (Heidelberg Engineering). If not detected by the system, the fovea was manually centered at the baseline visit. The built-in follow-up mode was used thereafter to reacquire follow-up scans. A registered 30-degree infrared image with a resolution of 768×768 pixels was acquired simultaneously with the OCT via the scanning laser ophthalmoscopy mode of the instrument. Thirty-degree FAF images (768×768 pixels) were acquired after OCT imaging in the same session after pupil dilation with 0.5% tropicamide and 2.5% phenylephrine to at least 6 mm diameter.

• **IMAGE PROCESSING AND BIOMARKER QUANTIFICATION:** HRF voxels were detected and segmented in a 3-dimensional (3D) OCT volume using a custom-built and validated DL algorithm based on a residual U-NET semantic segmentation architecture that was trained on a dataset consisting of images from patients with AMD, diabetic macular edema, and retinal vein occlusion. The algorithm has been validated and described in detail.[39]

The bright appearance of retinal vessels on OCT images may result in false-positive identification of HRF at vessel sites. The following procedure was implemented to filter out these false-positives to allow precise point-to-point assessment. After detection on infrared images, retinal vessels were transferred to the OCT scan using a custom-built registration algorithm.[47] To account for minor registration errors, the retinal vessels were enhanced by one hundredth of the 30-degree infrared image's side. A component filtering algorithm was applied to allow correct identification of retinal vessels and false-positive vessels were removed. All HRF colocalizing with retinal vessels on the en face image were subsequently removed, leaving only true HRF for evaluation (Figure 1). Each pixel of

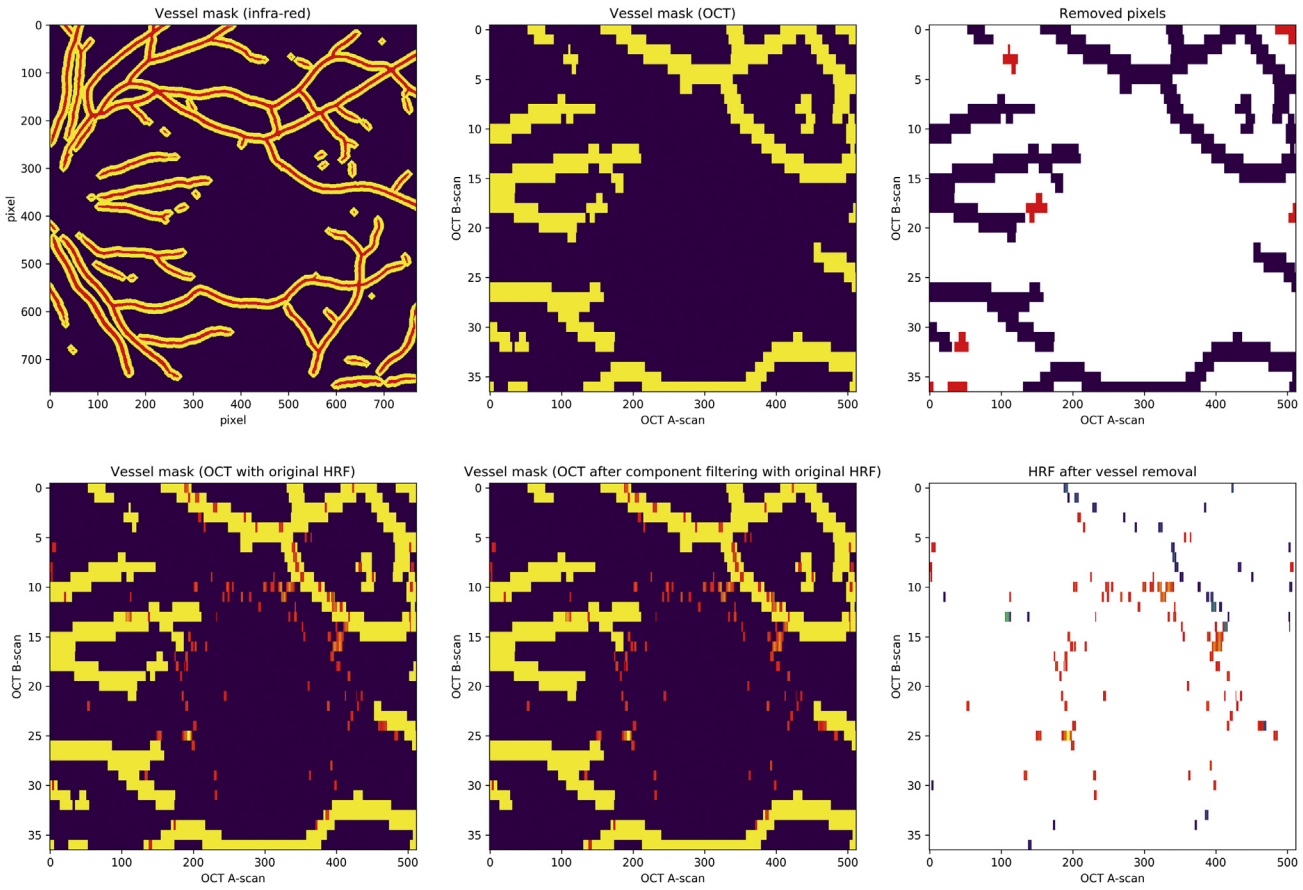

FIGURE 1. Retinal vessel identification and removal of false-positive hyperreflective foci (HRF) signals. Top left: Identification of retinal vessels (red) on the infrared image and thickening of the vessels (yellow) by 1% of the image's height. Top middle: Retinal vessels after registration to the optical coherence tomography (OCT) image. Top right: Removal of false-positive vessel signals (red) on the OCT scan. Bottom left: Overlay of retinal vessels (yellow) with HRF (red) before vessel filtering. Bottom middle: Retinal vessels (yellow) with overlying HRF (red) after component filtering. Bottom right: Separation of true positive HRF (red to yellow dashes, depending on each HRF A-scan length) and false-positive HRF signals (blue).

the individual en face HRF thickness map was color-coded by its size along the OCT A-scan (Figure 2).

GA lesions were delineated by certified graders (C.G., P.B.) on FAF images, which is to date the standard procedure for evaluating GA growth approved by the U.S. Food and Drug Administration.[48] The area of the GA that was annotated on FAF was then transferred to the OCT using the registration algorithm.[47]

A fixed custom junctional zone surrounding the GA lesion was then defined. This study used a 500-μm-wide parallel ring around the GA border for the spatial correlation of HRF to the GA border at baseline. Two-dimensional (2D) and 3D concentrations of HRF were calculated as the area and volume of pixels covered by HRF divided by the area of the region of interest (Figure 2).

• **STATISTICAL ANALYSIS:** Histograms were drawn to identify the distribution of data. All data were then calculated as the median (interquartile range [IQR]) if not normally distributed or mean ± standard deviation otherwise. Distances of HRF from the GA lesion were measured, including the distance of all individual HRF pixels from the immediate edge of the GA.

The intra-individual difference in HRF concentration between the growth area, defined as the difference between GA areas among 2 consecutive visits and the intact reference zone of 500 μm, was investigated with a Wilcoxon signed rank test computed for distribution of differences of HRF concentration between the corresponding areas. This was done separately for unifocal and multifocal lesions, as well as for the 2D and 3D concentrations of HRF. De novo GA development in areas with high concentrations of HRF were analyzed by comparing 2 regions of interest: the region where new GA appeared within 6 months and the region where no GA appeared in 6 months. The distributions of differences in HRF concentration were computed separately for 2D and 3D concentrations of HRF as well as for unifocal and multifocal lesions. Wilcoxon signed rank tests were performed to investigate whether these distributions were symmetrical around zero.

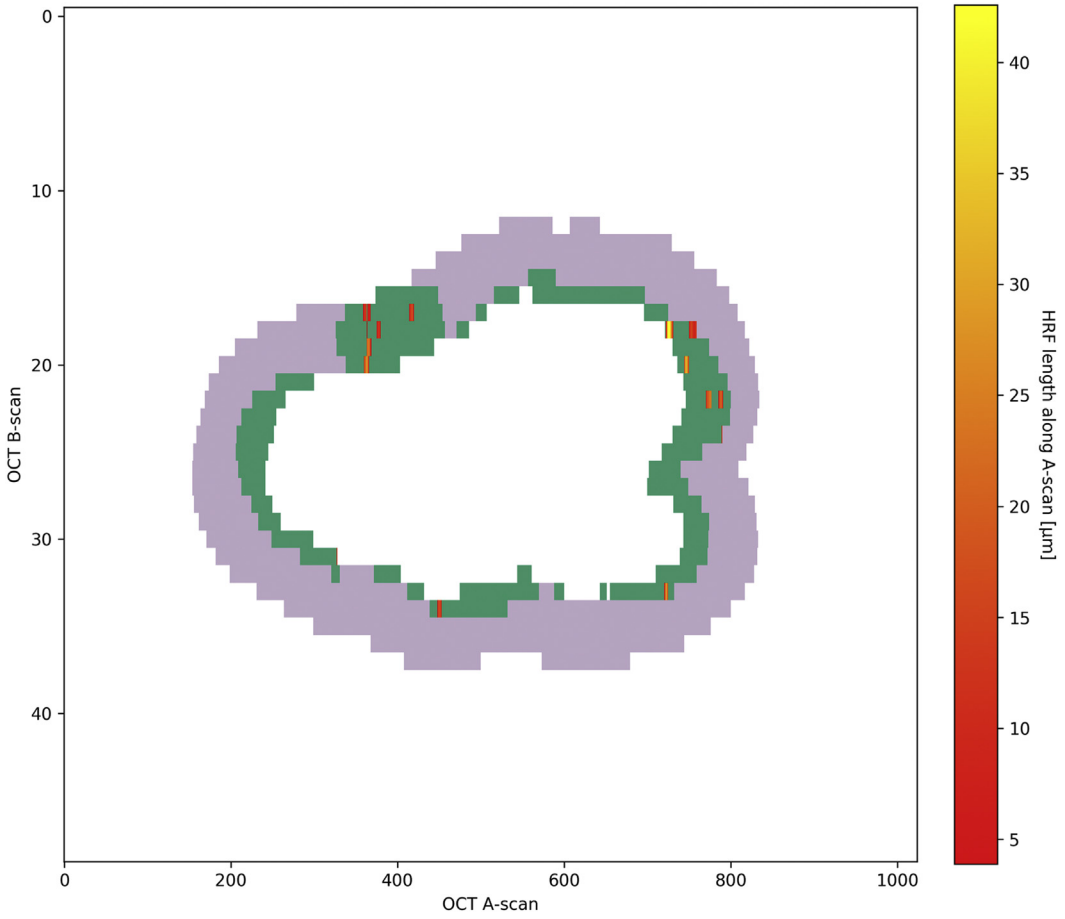

FIGURE 2. Delineated unifocal geographic atrophy (GA) after registration to the optical coherence tomography (OCT) image. A 500-µm-wide junctional zone (gray) was drawn along GA borders. The growth area was defined as the difference in GA extension between 2 consecutive 6-monthly visits (green). Hyperreflective foci (HRF, red to yellow dashes) were quantified within the junctional zone and color coded depending on the OCT A-scan length of each en face HRF signal.

To calculate the progression of GA in each eye, the GA area (assessed on FAF images) and the time difference to the first visit were considered for each consecutive visit. A linear regression was performed and the progression rate calculated as the slope of the fitted line. A central area with a radius of 1 mm around the center of the fovea was excluded from further analysis to account for the effect that GA lesions progress slower toward the fovea than the periphery[49] (Figure 3). The correlation between global GA progression (as assessed on FAF) and 2D and 3D HRF concentration in the junctional zone was then calculated using Spearman correlation coefficients. These were calculated for the HRF concentrations at baseline as well as for the HRF concentrations averaged over the entire follow-up period.

The correlation between local GA progression and HRF concentrations was assessed by assigning a circular region outside the atrophic area with a subjectively chosen radius of 800 µm to each pixel of the GA lesion's border. The count and concentration of HRF was assessed and normalized for each single circular region (Figure 4). To quantify local progression, each pixel of the GA rim (border) was assigned a value corresponding to the distance to the rim (border) of the GA lesion observed during the next visit. These values were then normalized (Figure 4). Spearman correlations were calculated to investigate the association between local GA growth and HRF counts and concentrations (both 2D and 3D).

Measures of local GA activity and local HRF activity were introduced to assess the correlation between local GA development and preceding HRF dynamics. For each pixel within the GA growth area between 2 visits, local GA activity was defined as the distance between that pixel and the rim (border) of the GA lesion observed during the earlier of the 2 visits under consideration. If a new GA lesion developed, all of its pixels were assigned a value corresponding to the radius of a circle with the same area (Figure 5). To describe HRF dynamics, en face HRF thickness maps were compared for pairs of consecutive visits. If the comparison was done in a pixel-wise manner, minor registration errors causing a shift in the position of the

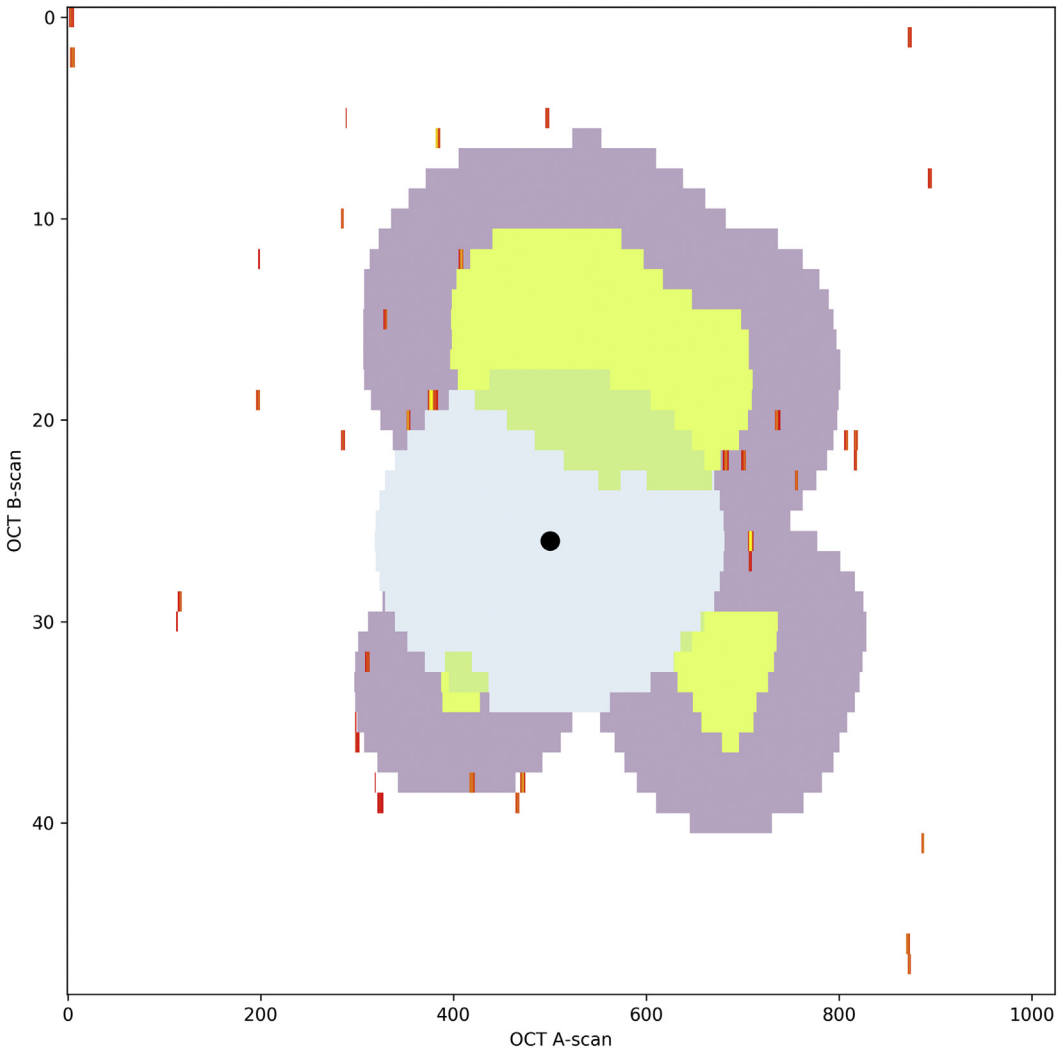

FIGURE 3. Delineation of multifocal geographic atrophy (GA). A 500-μm-wide junctional zone was drawn adjacent to the GA. The central 1 mm was excluded from analysis to account for the difference in directional progression speed. Hyperreflective foci (HRF) quantifications (red to yellow dashes) were co-registered to the optical coherence tomography (OCT) image.

same HRF between visits would result in detecting a false activity in 2 positions: disappearance of the HRF in the first position and appearance of the HRF in the second position. This issue was addressed by smoothening both en face maps: each pixel, instead of presenting HRF length along the corresponding A-scan, presented a mean of HRF lengths in the 500 μm × 500 μm square window centered at that pixel. Local HRF activity was defined for each pixel as an absolute difference between the values of corresponding pixels in the thus-defined maps (Figure 6). The groups of 3 consecutive visits were analyzed. The correlation between local HRF activity between the first 2 visits and local GA activity between the second 2 visits was quantified using Spearman correlation coefficient. The significance level for all calculations was set to $\alpha = 0.05$. No correction for multiple testing was performed for this explorative biomarker identification study.

RESULTS

• **DEMOGRAPHICS:** A total of 491 OCT volumes from 87 eyes of 54 patients with GA were included in this analysis. Median follow-up was 27.67 months (IQR: 14.03). Thirty-six eyes (41.4%) had unifocal and 51 eyes (58.6%) had multifocal GA lesions. The mean GA lesion size at baseline was 6.50 ± 5.24 mm^2. The mean progression of GA was 1.47 ± 1.12 mm^2/year. The mean age was 74.84 ± 8.01 years. Out of 54 patients, 34 (63%) were women. Detailed demographics separated for unifocal and multifocal GA are shown in Table 1.

• **DISTRIBUTION OF HYPERREFLECTIVE FOCI AT THE GEOGRAPHIC ATROPHY BORDER:** HRF distribution was found to be in close correlation with the GA border. The mean distance of HRF from the atrophy border was 860

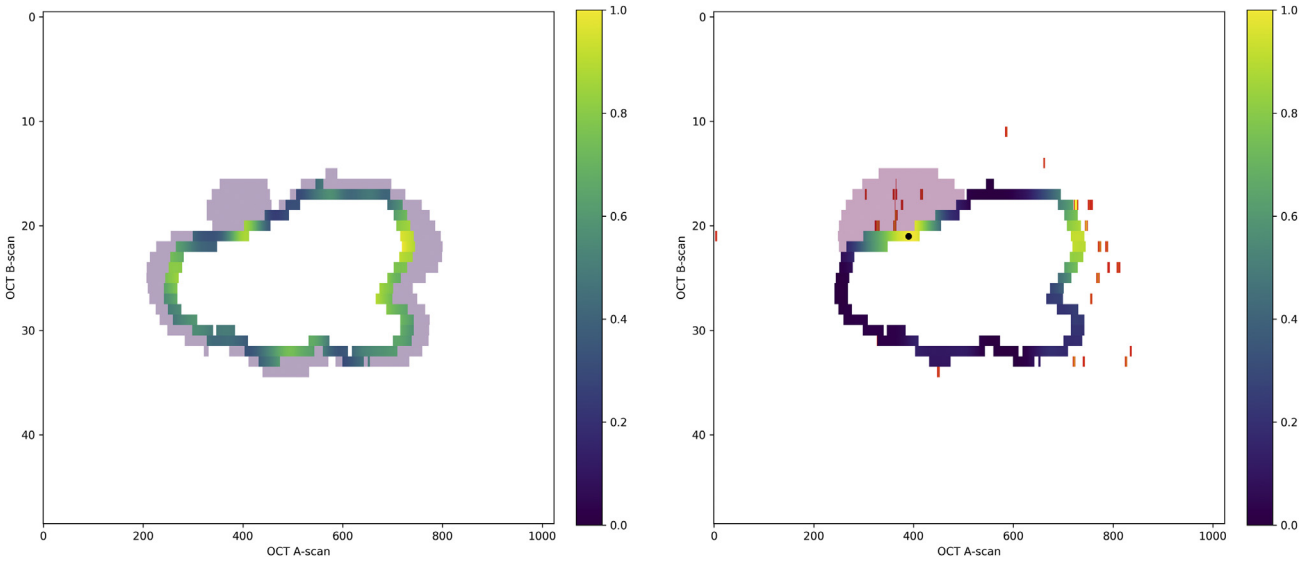

FIGURE 4. Left: Normalization of local geographic atrophy (GA) progression speed based on the amount of novel atrophic signals (gray). Higher values correspond to faster growth. Right: Concentration of hyperreflective foci (HRF, red to yellow dashes) within an 800-μm circle around each pixel of the GA border (exemplarily demonstrated as the pink circle with the black center dot). The higher the concentration of HRF in the circle, the higher the value at the GA border.

± 746 μm. Around two-thirds of all HRF were situated in a 1-mm junctional zone around the GA lesion. Detailed HRF distributions for unifocal and multifocal GA are shown in Table 2.

• **HYPERREFLECTIVE FOCI CONCENTRATION IN GEOGRAPHIC ATROPHY PROGRESSION:** Statistically significant differences were identified in the HRF concentration in the growth area compared with the remaining junctional zone in both unifocal GA (2D: $P < .001$; 3D: $P < .001$) and multifocal GA (2D: $P < .001$; 3D: $P < .001$). The median of 2D HRF concentration difference for unifocal and multifocal GA was 0.02 (IQR 0.02) and 0.01 (IQR 0.02), respectively. The 3D HRF concentration difference for unifocal and multifocal GA was 0.20 (IQR 0.29) and 0.13 (IQR 0.24), respectively (Figure 7).

• **HYPERREFLECTIVE FOCI CONCENTRATION PRECEDING GEOGRAPHIC ATROPHY DEVELOPMENT:** A statistically significant difference was found in the 2D HRF concentration between areas of GA development within the next 6 months and the area without new GA development within the next 6 months ($P = .037$). The difference was slightly above zero (median = 0.005, IQR: 0.043), indicating a higher concentration of 2D HRF in the areas next to develop GA. No statistical significance was found in the 3D HRF concentration between future GA and non-GA areas ($P = .058$) (Figure 8).

• **CORRELATION BETWEEN GEOGRAPHIC ATROPHY PROGRESSION AND HYPERREFLECTIVE FOCI CONCENTRATION:** Local progression of GA and local HRF concentrations as well as local HRF counts were assessed in relation to the GA lesion borders. Calculating Spearman correlation between the local GA progression and HRF concentration as well as HRF counts in unifocal GA, a significant positive correlation was found in 2D and 3D HRF concentrations (both $P < .001$, R = 0.09 [IQR: 0.21] and R = 0.08 [IQR: 0.2], respectively), as well as HRF counts ($P < .001$, R = 0.08 [IQR: 0.25] and $P = .003$, R = 0.06 [IQR: 0.18], respectively, Figure 9). Calculating Spearman correlations for multifocal GA, a significant average positive correlation was found between the local GA growth and 2D HRF concentrations and HRF counts ($P = .004$, R = 0.06 [IQR: 0.2] and $P = .002$, R = 0.06 [IQR: 0.25], respectively, Figure 9). No association was found in multifocal GA investigating the correlation between 3D HRF concentrations and counts with local GA progression (both $P > .05$, Figure 9).

Mean global GA progression was 1.47 ± 1.12 mm^2/year. Using the baseline 2D and 3D HRF concentrations, no significant correlation was found between the global GA progression and HRF concentrations in unifocal or multifocal lesions (all $P > .05$). When investigating the 2D and 3D HRF concentrations using the averaged HRF quantifications, no significant correlation was found between the global GA progression and the averaged HRF concentrations (all $P > .05$).

• **HYPERREFLECTIVE FOCI DYNAMICS BEFORE GEOGRAPHIC ATROPHY ACTIVITY:** Local HRF dynamics owing to length changes of HRF in the OCT A-scans

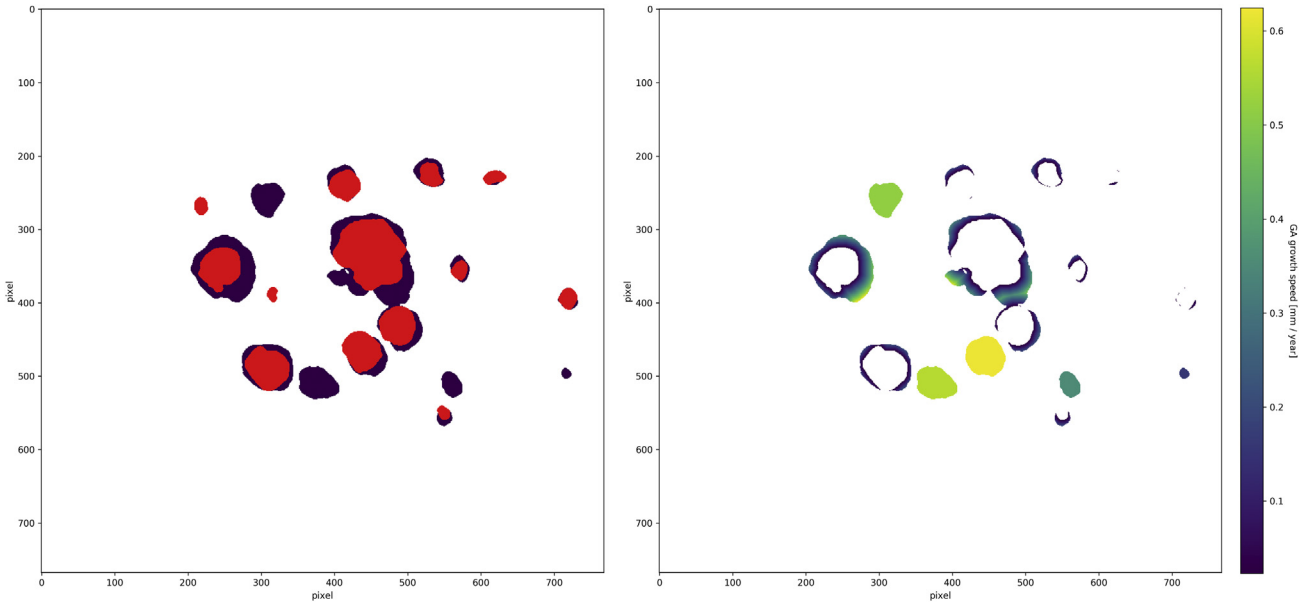

FIGURE 5. Assessment of local geographic atrophy (GA) speed and the normalization of de novo GA lesions. Left: The difference between 2 consecutive 6-monthly visits (first visit, red; second visit, purple) was defined as the growth area. Right: The growth area of a GA lesion was normalized based on the amount of pixel difference between 2 consecutive 6-monthly visits. Any de novo GA lesion was normalized and all of its pixels were assigned a value corresponding to the radius of a circle with the same area.

were assessed and an association with subsequent local GA activity after 6 months was investigated. No significant correlation was found between HRF dynamics and subsequent GA activity in either unifocal or multifocal GA lesions (both $P > .05$).

DISCUSSION

AI IS CURRENTLY SUCCESSFULLY IMPLEMENTED IN RETINAL diagnostics: It is now possible to correctly quantify retinal biomarkers on various imaging modalities and provide these tools for research and, eventually, individualized patient care.[3] Large digital datasets can be analyzed by automated algorithms in a fraction of the time that a human reader or retinal expert would require. This advantage on a large analysis scale offers a deeper understanding of diseases.[1] In macular diseases and pathologic aging, particularly AMD, various imaging biomarkers can be defined and, most importantly, quantified for investigation of their predictive values in disease progression. Apart from robust retinal layer segmentation and the precise spatial differentiation and quantification of retinal fluid compartments,[50–52] more refined biomarkers on a subclinical level, such as ellipsoid zone thickness or HRF, and the interaction of these biomarkers can now be explored to assess individual risk in disease progression.[16,53–56] The possibilities in AI are continuously expanding and novel, clinically unknown biomarkers can be identified using unsupervised learning. The latter lets the AI algorithm detect retinal markers on its own and evaluates them for the prediction of disease progression, which widely opens the spectrum of pathologic feature detection.[57]

In this study, a deep learning algorithm that allows spatial and temporal quantification of HRF in late AMD, showing a statistically significant association between the spatial presence of HRF and the local growth of GA, was applied. The majority of HRF derive from the junctional zone in close proximity to the GA lesion border. The accumulation of HRF predicts local progression of the atrophic lesion and indicates where and whether the atrophic lesion will expand. Contrary to the local prediction, a global prediction of GA progression was not possible. HRF density increased in areas of future multifocal GA lesions. However, no association was found between the dynamics of HRF before GA progression and the new development of GA lesions.

The junctional zone surrounding a GA lesion is prone to become atrophic during the natural course of disease progression.[25] To date, no drug slowing or inhibiting an atrophic lesion's growth has been approved for the treatment of GA secondary to AMD.[11] Correctly identifying patients and lesions that are at high risk of progression is therefore of great interest to plan therapeutic studies tailored to patients' disease stage. RPE in AMD is characterized by loss of intracellular granules and cytoskeleton derangements.[58] During disease progression of non-neovascular AMD, loss of RPE integrity is already detectable by the reduced quantitative autofluorescence in eyes with AMD compared with

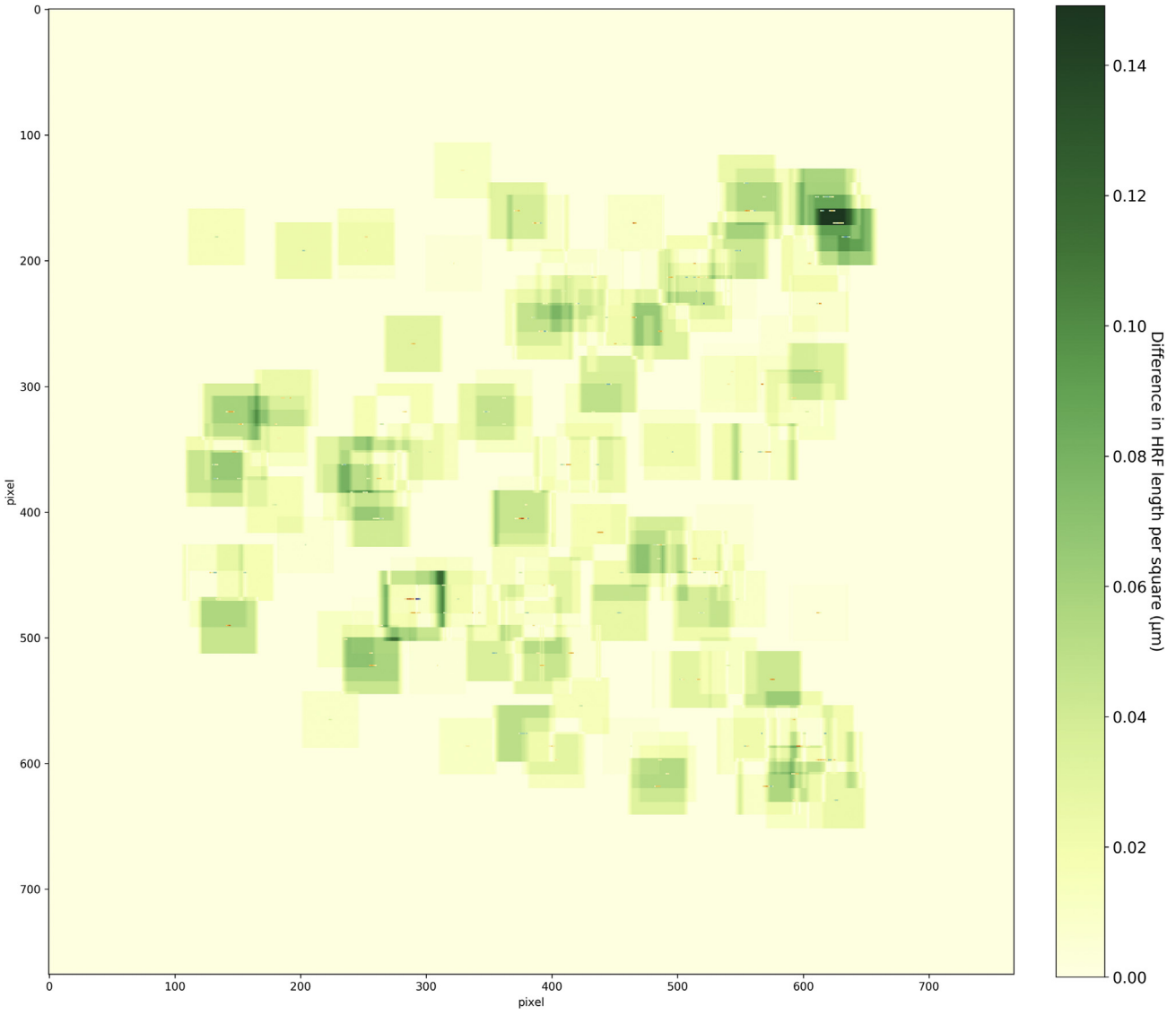

FIGURE 6. Dynamics of hyperreflective foci (HRF). Optical coherence tomography (OCT) A-scan length was defined for each HRF and the difference between 2 consecutive 6-monthly visits was assessed under the consideration of minor registration errors within 500-µm-sided squares. The amount of HRF dynamics within each square was then normalized.

healthy control eyes.[59] Above drusen the break-up of RPE can be visualized using exploratory polarization-sensitive OCT.[60] A close correlation between the size of a druse and alterations in the RPE can also be detected using this experimental technique,[61] and at the same time the segregation of HRF from the RPE can be visualized and the polarization of HRF indicates the origin from the RPE, which confirms SDOCT and histopathologic findings.[13,35,61] A correlation between the size of a drusenoid pigment epithelium detachment and a higher frequency of overlying hyperpigmentary alterations was described in the AREDS2 study, in which color fundus photography was used.[62] Using automated quantification of HRF on routine SDOCT, a correlation between HRF and the progression to late AMD, in particular atrophic AMD, was found.[21] Using multimodal imaging in combination with novel analytical tools from AI, it becomes evident that AMD follows the pathognomonic pathway of continuous RPE dysmorphia followed by intraretinal migration with progressive death of RPE cells and overlying photoreceptors.[63]

During disease progression in non-neovascular late AMD, the nonatrophic junctional zone in GA presents various alterations in histology, such as photoreceptor shortening, dysmorphic RPE, and a dyslaminated outer nuclear layer.[32,64] A hyporeflective wedge becomes visible on OCT that corresponds to a Henle fiber layer without cellular infiltration.[32,65] Müller cells irrupt into the sub-RPE space and might play an important role during the

TABLE 1. Demographic Summary Collected From 87 Study Eyes

Demographics	Any GA	Unifocal GA	Multifocal GA
Eyes, n (%)	87 (100)	36 (41.4)	51 (58.6)
Age (years), mean (SD)	74.84 (8.01)	76.11 (8.18)	74.02 (7.88)
Female sex, n (%) eyes	56 (64.4)	25 (69.4)	31 (60.8)
Baseline GA area (mm^2)	6.50 (5.24)	7.34 (5.90)	5.90 (4.62)
Follow-up period (months), median (IQR)	27.67 (14.03)	28.67 (6.95)	25.87 (18.43)

GA = geographic atrophy; IQR = interquartile range.

TABLE 2. Distribution of Hyperreflective Foci in Relation to the Geographic Atrophy Lesion Border

	Any GA		Unifocal GA		Multifocal GA	
Junctional Zone Ring (μm)	% per Ring	Cumulative %	% per Ring	Cumulative %	% per Ring	Cumulative %
1-250	25	25	26	26	25	25
251-500	16	41	14	39	17	42
501-750	14	55	12	51	15	57
751-1000	10	65	12	63	10	66
1001-1500	14	79	17	79	13	79
1501-2000	12	91	11	91	12	91
2001-2500	6	97	6	97	6	97
2501-	3	100	4	100	3	100

GA = geographic atrophy.

enlargement of GA with the concurrent formation of outer retinal tubulations.[66,67] Müller cell contribution to HRF features have been described as well.[68,69] The damage to the RPE in the junctional zone in GA is already remarkable with reduced intracellular autofluorescence alone.[34,35] A delineation by an adjacent hyperautofluorescent rim might indicate an increase in cellular RPE damage[70]; however, the general quantitative autofluorescence in the junctional zone is already decreased in patients with solitary GA,[33] supporting the pathomechanism of continuous loss of RPE and its fluorophores during disease progression.[58,71] The formation and migration of HRF into the inner retinal layers accompanies continuous RPE loss.[13] In this study, this concomitant process can be seen on OCT with the accumulation of HRF close to the GA border (mean HRF distance: 860 ± 746 μm), with the majority of HRF present within the millimeter adjacent to the GA border (approximately 65%), as seen by automated counting. Furthermore, not only were HRF abundantly present close to the GA border but the concentration of HRF was also higher in future GA lesion areas than in nongrowing areas within a 500-μm junctional zone ($P < .001$ for both 2D and 3D HRF concentration). The 2D concentration of HRF was also significantly higher in areas where a new GA lesion will develop at least 6 months later compared with the area where no GA occurs ($P = .037$). However, only 2D concentrations of HRF reached significance, while 3D concentrations of HRF were close to being significantly different between these respective areas ($P = .058$). This is explained by the difficulty in monitoring individual HRF by SDOCT with a distance between B-scans larger than the HRF. Nonetheless, with a significant difference in 2D concentration (median = 0.005) and a trend toward higher 3D concentrations of HRF (median = 0.032), this hypothesis seems valid.

Individual regression slopes were calculated first to investigate the association of HRF with GA progression. The mean GA growth in this study was 1.47 ± 1.12 mm^2/year, which accords well with the literature.[30,31,72,73] However, no correlation was found between the 2D or 3D HRF concentrations and the global GA progression in either unifocal or multifocal lesions in this study. When assessing local progression speed with normalization of the GA border based on the 6-monthly growth speed and HRF concentrations, a significant positive correlation between the 2D and 3D HRF concentrations and HRF counts in unifocal GA was found (all $P < .001$, except 3D count $P = .003$). This result indicates that unifocal GA progresses faster with higher concentrations of HRF near the border of atrophy. In multifocal GA, a significant

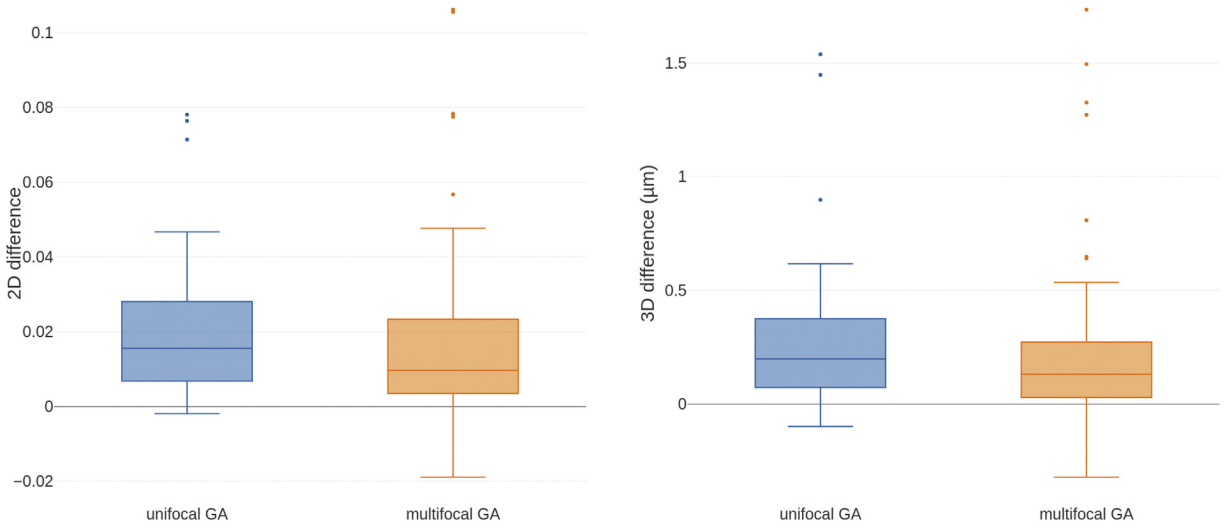

FIGURE 7. Distribution of differences between 2-dimensional (2D) (left pair) and 3-dimensional (3D) (right pair) concentrations of hyperreflective foci (HRF) within the 500-µm junctional zone around the geographic atrophy (GA) lesion. The significance in differences between future growth areas and non-growth areas was calculated using Wilcoxon signed rank tests. All calculations resulted in a statistically significant difference with, on average, higher HRF concentration in future growth areas (all $P < .001$).

positive correlation was only found between the 2D HRF concentrations and counts with GA growth ($P = .004$ and $P = .002$, respectively). These results indicate faster progression with higher HRF concentration, assuming that HRF are already present at the time of assessment. The stated correlation coefficients were not very high, but were statistically significant even in a relatively small cohort, which indicates that HRF quantifications indeed have a relevant association with local GA growth. However, HRF are not the only imaging biomarker associated with GA growth, and the interactions of all related biomarkers remains to be assessed in a larger dataset. In general, distinct and pathophysiologically evident biomarkers such as HRF are easy to measure by AI tools and would therefore offer good utility in clinical practice. When assessing another dimension, HRF dynamics over time, and the association between HRF dynamics with GA progression speed, no such correlation was found ($P > .05$ for both unifocal and multifocal GA). In a spatial correlation, HRF are therefore close to the border of atrophy and indicators of RPE cell death in the junctional zone. Preceding GA progression in a temporal dimension, HRF might already be present and the local dynamics of HRF do not affect overall GA progression.

The advantages of this study lie in the quantification of HRF using a validated DL algorithm[39] and the automated registration of different retinal imaging modalities such as SDOCT and FAF, which allows precise intra-individual monitoring of subclinical biomarkers such as HRF with high agreement.[47,74] Another benefit is the long and standardized follow-up of over 27 months (IQR: 14.03), which allows precise detection of GA growth as well as de novo

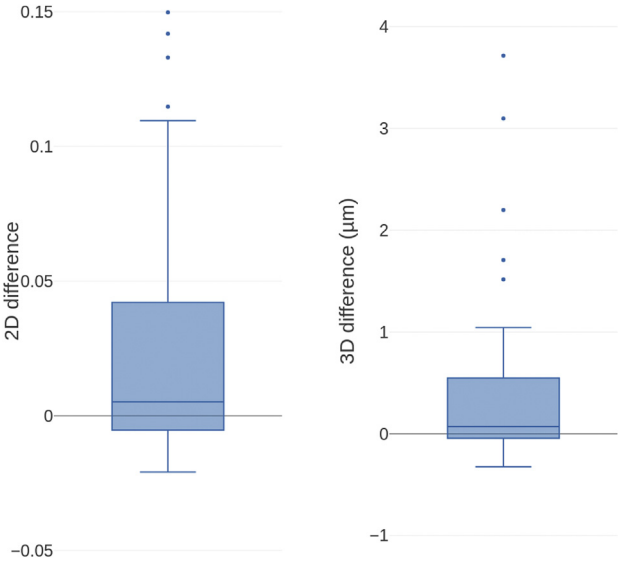

FIGURE 8. Distribution of differences between 2-dimensional (2D) (left) and 3-dimensional (3D) (right) concentrations of hyperreflective foci (HRF) within de novo geographic atrophy areas in the next 6 months. A significantly higher 2D HRF concentration was found in areas that will develop GA in 6 months or earlier ($P = .037$). No significant difference was found with 3D HRF concentrations ($P > .05$).

GA development. We showed that the majority of HRF accumulate in the immediate area around the GA lesion. However, very distant HRF might have not been detected owing to the 20-degree OCT imaging protocol and this has to be accepted as a limitation. This study focused on the

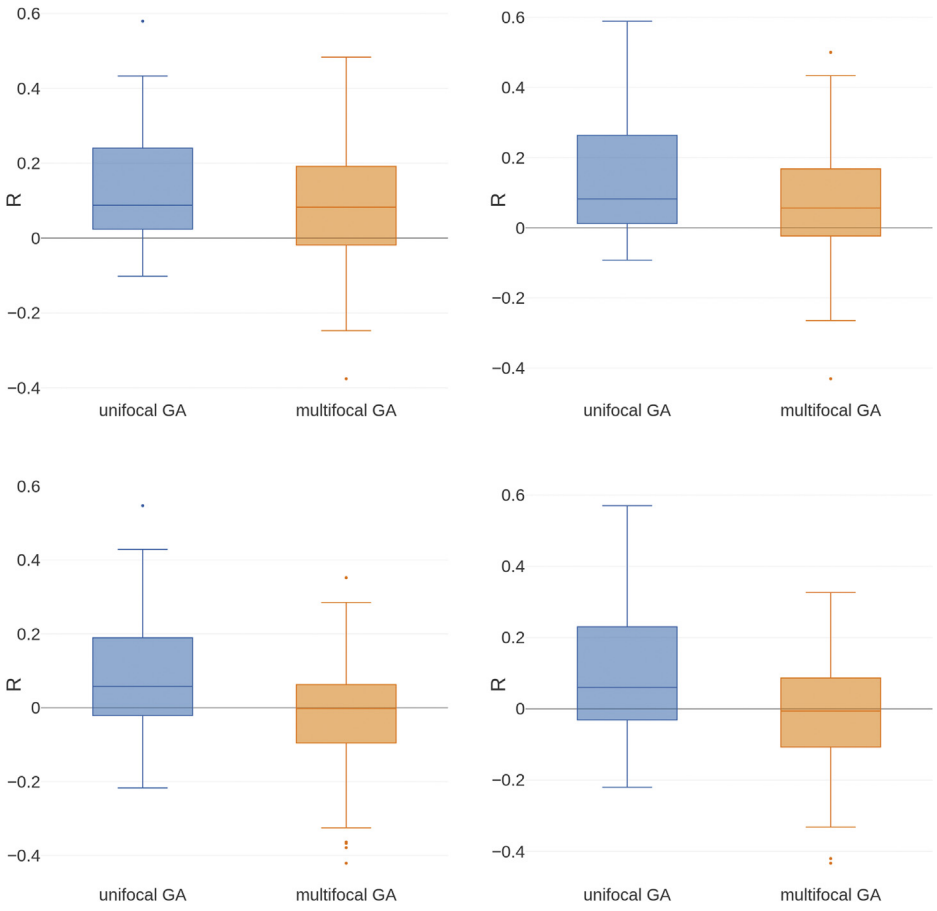

FIGURE 9. Distribution of Spearman correlation between local geographic atrophy (GA) progression and hyperreflective foci (HRF) concentrations and counts for unifocal (blue) and multifocal (orange) lesions. Top left pair: Correlations of local GA progression and 2-dimensional (2D) HRF concentration. Top right pair: Correlations of local GA progression and 3-dimensional (3D) HRF concentrations. Bottom left pair: Correlations of local GA progression and 2D HRF counts. Bottom right pair: Correlations of local GA progression and 3D HRF counts. All mean correlations reached statistical significance, except 2D and 3D HRF counts in multifocal GA.

quantification of HRF and investigation of HRF as a predictive biomarker in GA. Other predictive OCT findings that may accelerate global and local GA progression such as subretinal drusenoid deposits can also be found at the same time.[75] Owing to the exploratory nature of the study, all available eyes were included in our analysis without accounting for within-subjects factors. As part of future work, the interactions with other imaging biomarkers and correlations between fellow eyes will be accounted for in a larger dataset. Another limitation of this study is the 6-monthly image acquisition, as subtler changes might have been detectable with more frequent study visits, a higher number of included eyes, or denser OCT volume scans. However, as GA progression is slow, the focus of this study was set on prospective longitudinal data with appropriate follow-up using a deep learning algorithm validated for patients with AMD, diabetic macular edema, and retinal vein occlusion in a solid manner.

In summary, applying a deep learning algorithm for HRF quantification to a standardized clinical GA population, we could demonstrate that HRF are more frequent close to the active border of a lesion. Not only are the concentrations of HRF higher in areas of future GA progression, but HRF accumulation is also higher in areas with future de novo GA development. Investigating global and local progression speed, no association of HRF with global GA progression was found; however, local progression speed of GA was on average positively correlated with HRF quantifications, indicating faster progression with higher HRF presentation. Through quantifications of HRF, areas with irreversible RPE alterations can be identified and the association with disease progression provides evidence of virulent RPE death in AMD. AI provides a valuable tool for identifying and correctly quantifying even subclinical retinal biomarkers. New approaches such as unsupervised learning are expected to open the horizon to novel biomarker detection not visible to the physician's eye and provide a fast, reliable, and inexpensive approach to individualized patient care with objective decision-making and clear guidance.

FUNDING/SUPPORT: NO FUNDING OR GRANT SUPPORT.
Financial Disclosures: Ursula Schmidt-Erfurth: Consultancy (Boehringer Ingelheim, Novartis, Roche, Genentech, Kodiak); Sebastian Waldstein: Consultancy (Novartis), Research support (Bayer, Genentech). The following authors have no financial disclosures: Hrvoje Bogunovic, Christoph Grechenig, Patricia Bui, Maria Fabianska, and Gregor S. Reiter. All authors attest that they meet the current ICMJE criteria for authorship.

REFERENCES

1. Jiang F, Jiang Y, Zhi H, et al. Artificial intelligence in healthcare: past, present and future. *Stroke Vasc Neurol* 2017;2(4):230–243.
2. Schmidt-Erfurth U, Klimscha S, Waldstein SM, Bogunović H. A view of the current and future role of optical coherence tomography in the management of age-related macular degeneration. *Eye* 2017;31(1):26–44.
3. Schmidt-Erfurth U, Sadeghipour A, Gerendas BS, Waldstein SM, Bogunović H. Artificial intelligence in retina. *Prog Retin Eye Res* 2018;67:1–29.
4. Wong WL, Su X, Li X, et al. Global prevalence of age-related macular degeneration and disease burden projection for 2020 and 2040: a systematic review and meta-analysis. *Lancet Glob Heal* 2014;2(2):e106–e116.
5. Ferris FL, Wilkinson CP, Bird A, et al. Clinical classification of age-related macular degeneration. *Ophthalmology* 2013;120(4):844–851.
6. Mitchell P, Liew G, Gopinath B, Wong TY. Age-related macular degeneration. *Lancet* 2018;392(10153):1147–1159.
7. Spaide RF. Improving the age-related macular degeneration construct. *Retina* 2018;38(5):891–899.
8. Sunness JS. The natural history of geographic atrophy, the advanced atrophic form of age-related macular degeneration. *Mol Vis* 1999;5:25.
9. Bonilha VL. Age and disease-related structural changes in the retinal pigment epithelium. *Clin Ophthalmol* 2008;2(2):413–424.
10. Sayegh RG, Sacu S, Dunavölgyi R, et al. Geographic atrophy and foveal-sparing changes related to visual acuity in patients with dry age-related macular degeneration over time. *Am J Ophthalmol* 2017;54:739–745.
11. Boyer DS, Schmidt-Erfurth U, van Lookeren Campagne M, Henry EC, Brittain C. The pathophysiology of geographic atrophy secondary to age-related macular degeneration and the complement pathway as a therapeutic target. *Retina* 2017;37(5):819–835.
12. Schlanitz FG, Baumann B, Kundi M, et al. Drusen volume development over time and its relevance to the course of age-related macular degeneration. *Br J Ophthalmol* 2017;101(2):198–203.
13. Curcio CA, Zanzottera EC, Ach T, Balaratnasingam C, Freund KB. Activated retinal pigment epithelium, an optical coherence tomography biomarker for progression in age-related macular degeneration. *Invest Ophthalmol Vis Sci* 2017;58(6):BIO211–BIO226.
14. de Sisternes L, Simon N, Tibshirani R, Leng T, Rubin DL. Quantitative SD-OCT imaging biomarkers as indicators of age-related macular degeneration progression. *Invest Ophthalmol Vis Sci* 2014;55(11):7093–7103.
15. Tan ACS, Pilgrim MG, Fearn S, et al. Calcified nodules in retinal drusen are associated with disease progression in age-related macular degeneration. *Sci Transl Med* 2018;10(466):eaat4544.
16. Schmidt-Erfurth U, Waldstein SM, Klimscha S, et al. Prediction of individual disease conversion in early AMD using artificial intelligence. *Invest Ophthalmol Vis Sci* 2018;59(8):3199–3208.
17. Bogunovic H, Montuoro A, Baratsits M, et al. Machine learning of the progression of intermediate age-related macular degeneration based on OCT imaging. *Invest Ophthalmol Vis Sci* 2017;58(6):BIO141–BIO150.
18. Lei J, Balasubramanian S, Abdelfattah NS, Nittala MG, Sadda SR. Proposal of a simple optical coherence tomography-based scoring system for progression of age-related macular degeneration. *Graefes Arch Clin Exp Ophthalmol* 2017;255(8):1551–1558.
19. Schaal KB, Gregori G, Rosenfeld PJ. En face optical coherence tomography imaging for the detection of nascent geographic atrophy. *Am J Ophthalmol* 2017;174:145–154.
20. Sleiman K, Veerappan M, Winter KP, et al. Optical coherence tomography predictors of risk for progression to non-neovascular atrophic age-related macular degeneration. *Ophthalmology* 2017;124(12):1764–1777.
21. Nassisi M, Fan W, Shi Y, et al. Quantity of intraretinal hyperreflective foci in patients with intermediate age-related macular degeneration correlates with 1-year progression. *Invest Ophthalmol Vis Sci* 2018;59(8):3431–3439.
22. Ouyang Y, Heussen FM, Hariri A, Keane PA, Sadda SR. Optical coherence tomography-based observation of the natural history of drusenoid lesion in eyes with dry age-related macular degeneration. *Ophthalmology* 2013;120(12):2656–2665.
23. Christenbury JG, Folgar FA, O'Connell RV, et al. Progression of intermediate age-related macular degeneration with proliferation and inner retinal migration of hyperreflective foci. *Ophthalmology* 2013;120(5):1038–1045.
24. Gambril JA, Sloan KR, Swain TA, et al. Quantifying retinal pigment epithelium dysmorphia and loss of histologic autofluorescence in age-related macular degeneration. *Invest Ophthalmol Vis Sci* 2019;60(7):2481.
25. Sarks JP, Sarks SH, Killingsworth MC. Evolution of geographic atrophy of the retinal pigment epithelium. *Eye* 1988;2(5):552–577.
26. Balaratnasingam C, Yannuzzi LA, Curcio CA, et al. Associations between retinal pigment epithelium and drusen volume changes during the lifecycle of large drusenoid pigment epithelial detachments. *Invest Ophthalmol Vis Sci* 2016;57(13):5479–5489.
27. Folgar FA, Chow JH, Farsiu S, et al. Spatial correlation between hyperpigmentary changes on color fundus photography and hyperreflective foci on SDOCT in intermediate AMD. *Invest Ophthalmol Vis Sci* 2012;53(8):4626–4633.
28. Ho J, Witkin AJ, Liu J, et al. Documentation of intraretinal retinal pigment epithelium migration via high-speed

ultrahigh-resolution optical coherence tomography. *Ophthalmology* 2011;118(4):687–693.
29. Davis MD, Gangnon RE, Lee L-Y, et al. The Age-Related Eye Disease Study severity scale for age-related macular degeneration: AREDS Report No. 17. *Arch Ophthalmol* 2005; 123(11):1484–1498.
30. Yehoshua Z, Rosenfeld PJ, Gregori G, et al. Progression of geographic atrophy in age-related macular degeneration imaged with spectral domain optical coherence tomography. *Ophthalmology* 2011;118(4):679–686.
31. Keenan TD, Agrón E, Domalpally A, et al. Progression of geographic atrophy in age-related macular degeneration: AREDS2 Report Number 16. *Ophthalmology* 2018;125(12): 1913–1928.
32. Li M, Dolz-Marco R, Huisingh C, et al. clinicopathologic correlation of geographic atrophy secondary to age-related macular degeneration. *Retina* 2019;39(4):802–816.
33. Reiter GS, Told R, Baumann L, Sacu S, Schmidt-Erfurth U, Pollreisz A. Investigating a growth prediction model in advanced age-related macular degeneration with solitary geographic atrophy using quantitative autofluorescence. *Retina* 2019; https://doi.org/10.1097/IAE.0000000000002653.
34. Rudolf M, Vogt SD, Curcio CA, et al. Histologic basis of variations in retinal pigment epithelium autofluorescence in eyes with geographic atrophy. *Ophthalmology* 2013;120(4): 821–828.
35. Zanzottera EC, Ach T, Huisingh C, Messinger JD, Spaide RF, Curcio CA. Visualizing retinal pigment epithelium phenotypes in the transition to geographic atrophy in age-related macular degeneration. *Retina* 2016;36(Suppl 1):S12–S25.
36. Allingham MJ, Nie Q, Lad EM, et al. Semiautomatic segmentation of rim area focal hyperautofluorescence predicts progression of geographic atrophy due to dry age-related macular degeneration. *Invest Ophthalmol Vis Sci* 2016;57(4): 2283–2289.
37. Hwang JC, Chan JWK, Chang S, Smith RT. Predictive value of fundus autofluorescence for development of geographic atrophy in age-related macular degeneration. *Invest Ophthalmol Vis Sci* 2006;47(6):2655–2661.
38. Qu J, Velaga SB, Hariri AH, Nittala MG, Sadda S. Classification and quantitative analysis of geographic atrophy junctional zone using spectral domain optical coherence tomography. *Retina* 2018;38(8):1456–1463.
39. Schlegl T, Bogunovic H, Klimscha S, et al. Fully automated segmentation of hyperreflective foci in optical coherence tomography images. arxiv Prepr; 2018. arXiv:18050327.
40. Sayegh RG, Simader C, Scheschy U, et al. A systematic comparison of spectral-domain optical coherence tomography and fundus autofluorescence in patients with geographic atrophy. *Ophthalmology* 2011;118(9):1844–1851.
41. Simader C, Sayegh RG, Montuoro A, et al. A longitudinal comparison of spectral-domain optical coherence tomography and fundus autofluorescence in geographic atrophy. *Am J Ophthalmol* 2014;158(3):557–566.
42. Schütze C, Ahlers C, Sacu S, et al. Performance of OCT segmentation procedures to assess morphology and extension in geographic atrophy. *Acta Ophthalmol* 2011;89(3):235–240.
43. Sayegh RG, Zotter S, Roberts PK, et al. Polarization-sensitive optical coherence tomography and conventional retinal imaging strategies in assessing foveal integrity in geographic atrophy. *Invest Ophthalmol Vis Sci* 2015;56(9):5246–5255.
44. Sayegh RG, Kiss CG, Simader C, et al. A systematic correlation of morphology and function using spectral domain optical coherence tomography and microperimetry in patients with geographic atrophy. *Br J Ophthalmol* 2014;98(8): 1050–1055.
45. Schütze C, Bolz M, Sayegh R, et al. Lesion size detection in geographic atrophy by polarization-sensitive optical coherence tomography and correlation to conventional imaging techniques. *Invest Opthalmol Vis Sci* 2013;54(1):739.
46. Reumueller A, Sacu S, Karantonis MG, Steiner I, Weigert G, Schmidt-Erfurth U. Semi-automated quantification of geographic atrophy with blue-light autofluorescence and spectral-domain optical coherence tomography: a comparison between the region finder and the advanced retinal pigment epithelium tool in the clinical setting. *Acta Ophthalmol* 2019;97(6):e887–e895.
47. Arikan M, Sadeghipour A, Gerendas B, Told R, Schmidt-Erfurth U. Deep learning based multi-modal registration for retinal imaging. In: Suzuki K, et al., eds. Interpretability of Machine Intelligence in Medical Image Computing and Multimodal Learning for Clinical Decision Support. Cham: Springer; 2019:75–82.
48. Sadda SR, Chakravarthy U, Birch DG, Staurenghi G, Henry EC, Brittain C. Clinical endpoints for the study of geographic atrophy secondary to age-related macular degeneration. *Retina* 2016;36(10):1806–1822.
49. Lindner M, Böker A, Mauschitz MM, et al. Directional kinetics of geographic atrophy progression in age-related macular degeneration with foveal sparing. *Ophthalmology* 2015; 122(7):1356–1365.
50. Montuoro A, Waldstein SM, Gerendas BS, Schmidt-Erfurth U, Bogunović H. Joint retinal layer and fluid segmentation in OCT scans of eyes with severe macular edema using unsupervised representation and auto-context. *Biomed Opt Express* 2017;8(3):1874.
51. Klimscha S, Waldstein SM, Schlegl T, et al. Spatial correspondence between intraretinal fluid, subretinal fluid, and pigment epithelial detachment in neovascular age-related macular degeneration. *Invest Ophthalmol Vis Sci* 2017; 58(10):4039–4048.
52. Schlegl T, Waldstein SM, Bogunovic H, et al. Fully automated detection and quantification of macular fluid in OCT using deep learning. *Ophthalmology* 2018;125(4): 549–558.
53. Orlando JI, Seebock P, Bogunovic H, et al. U2-Net: A Bayesian U-Net model with epistemic uncertainty feedback for photoreceptor layer segmentation in pathological OCT scans. 2019 IEEE 16th International Symposium on Biomedical Imaging (ISBI 2019). Vol 2019-April. IEEE; 2019;:1441–1445.
54. Orlando JI, Breger A, Bogunović H, et al. An amplified-target loss approach for photoreceptor layer segmentation in pathological OCT scans. In: Fu H, Garvin M, MacGillivray T, Xu Y, Zheng Y, eds. Ophthalmic Medical Image Analysis. OMIA 2019. Lecture Notes in Computer Science. Cham: Springer; 2019:26–34.
55. Rivail A, Schmidt-Erfurth U, Vogl W-D, et al. Modeling disease progression in retinal OCTs with longitudinal self-supervised learning. In: Rekik I, Adeli E, Park S, eds. Predictive

Intelligence in Medicine. PRIME 2019. Lecture Notes in Computer Science. Cham: Springer; 2019:44–52.
56. Riedl S, Cooney L, Grechenig C, et al. Topographic analysis of photoreceptor loss correlated with disease morphology in neovascular age-related macular degeneration. *Retina* 2019; https://doi.org/10.1097/IAE.0000000000002717.
57. Seebock P, Waldstein SM, Klimscha S, et al. Unsupervised identification of disease marker candidates in retinal OCT imaging data. *IEEE Trans Med Imaging* 2018;38:1037–1047.
58. Ach T, Tolstik E, Messinger JD, Zarubina AV, Heintzmann R, Curcio CA. Lipofuscin redistribution and loss accompanied by cytoskeletal stress in retinal pigment epithelium of eyes with age-related macular degeneration. *Invest Ophthalmol Vis Sci* 2015;56(5):3242–3252.
59. Orellana-Rios J, Yokoyama S, Agee JM, et al. Quantitative fundus autofluorescence in non-neovascular age-related macular degeneration. *Ophthalmic Surg Lasers Imaging Retina* 2018; 49(10):S34–S42.
60. Pircher M, Hitzenberger CK, Schmidt-Erfurth U. Polarization sensitive optical coherence tomography in the human eye. *Prog Retin Eye Res* 2011;30(6):431–451.
61. Schlanitz F, Baumann B, Sacu S, et al. Impact of drusen and drusenoid retinal pigment epithelium elevation size and structure on the integrity of the retinal pigment epithelium layer. *Br J Ophthalmol* 2019;103(2):227–232.
62. Yu JJ, Agrón E, Clemons TE, et al. Natural history of drusenoid pigment epithelial detachment associated with age-related macular degeneration. *Ophthalmology* 2019;126(2): 261–273.
63. Mrejen S, Sarraf D, Mukkamala SK, Freund KB. Multimodal imaging of pigment epithelial detachment: a guide to evaluation. *Retina* 2013;33:1735–1762.
64. Li M, Huisingh C, Messinger J, et al. Histology of geographic atrophy secondary to age-related macular degeneration. *Retina* 2018;38(10):1937–1953.
65. Monés J, Biarnés M, Trindade F. Hyporeflective wedge-shaped band in geographic atrophy secondary to age-related macular degeneration: an underreported finding. *Ophthalmology* 2012;119(7):1412–1419.
66. Preti RC, Govetto A, Filho RGA, et al. Optical coherence tomography analysis of outer retinal tubulations. *Retina* 2018;38(8):1518–1525.
67. Dolz-Marco R, Litts KM, Tan ACS, Freund KB, Curcio CA. The evolution of outer retinal tubulation, a neurodegeneration and gliosis prominent in macular diseases. *Ophthalmology* 2017;124(9):1353–1367.
68. Midena E, Pilotto E. Emerging insights into pathogenesis. *Dev Ophthalmol* 2017;60:16–27.
69. Pilotto E, Midena E, Longhin E, Parrozzani R, Frisina R, Frizziero L. Müller cells and choriocapillaris in the pathogenesis of geographic atrophy secondary to age-related macular degeneration. *Graefes Arch Clin Exp Ophthalmol* 2019; 257(6):1159–1167.
70. Shen LL, Liu F, Nardini HG, Del Priore LV. Reclassification of fundus autofluorescence patterns surrounding geographic atrophy based on progression rate. *Retina* 2019;39(10): 1829–1839.
71. Ach T, Best G, Rossberger S, Heintzmann R, Cremer C, Dithmar S. Autofluorescence imaging of human RPE cell granules using structured illumination microscopy. *Br J Ophthalmol* 2012;96(8):1141–1144.
72. Lindblad AS, Lloyd PC, Clemons TE, et al. Change in area of geographic atrophy in the Age-Related Eye Disease Study: AREDS report number 26. *Arch Ophthalmol* 2009;127(9): 1168–1174.
73. Uji A, Nittala MG, Hariri A, Velaga SB, Sadda SR. Directional kinetics analysis of the progression of geographic atrophy. *Graefes Arch Clin Exp Ophthalmol* 2019;257(8): 1679–1685.
74. Told R, Reiter GS, Orsolya A, et al. Swept source optical coherence tomography angiography, fluorescein angiography, and indocyanine green angiography comparisons revisited. *Retina* 2019; https://doi.org/10.1097/IAE.0000000000002695.
75. Reiter GS, Told R, Schranz M, et al. Subretinal drusenoid deposits and photoreceptor loss detecting global and local progression of geographic atrophy by SD-OCT imaging. *Invest Ophthalmol Vis Sci* 2020; https://doi.org/10.1167/iovs.0.0.29208.